Propagation of intense short laser pulses in a gas of atomic clusters

Ayush Gupta,[1] T. M. Antonsen, Jr.,[1] and H. M. Milchberg[2]
[1]*Department of Electrical and Computer Engineering and Institute of Research in Electronics and Applied Physics, University of Maryland, College Park, Maryland 20742, USA*
[2]*Department of Electrical and Computer Engineering and Institute for Physical Science and Technology, University of Maryland, College Park, Maryland 20742, USA*
(Received 19 January 2004; revised manuscript received 16 June 2004; published 25 October 2004)

We present a model and numerical simulations for the propagation of intense short laser pulses in gases of atomic clusters. As the pulse propagates through the clusters, they absorb energy, expand and explode. The clustered gas thus acts as a medium with time dependent effective dielectric constant. A self-consistent model for the cluster expansion and the laser pulse propagation is developed. Self-focusing of the laser pulse, coupling of laser energy to clusters and the evolution of the pulse spectrum are studied for a laser-cluster system with typical laboratory parameters.

DOI: 10.1103/PhysRevE.70.046410 PACS number(s): 52.38.Hb, 52.35.Mw, 42.65.Jx, 52.38.Dx

I. INTRODUCTION

A cluster is an aggregate of typically 10^2-10^6 atoms (usually of rare gases for example argon and helium) held together by Van der Waals forces. Clusters are formed when the rare gas, under controlled temperature and pressure conditions, is passed into a vacuum chamber. When irradiated by an intense laser pulse, clusters absorb energy and explode, leaving behind tenuous plasma. Gases of atomic clusters are an interesting media for laser-matter interaction with many applications such as generation of x rays [1] and extreme ultraviolet (EUV) radiation [2], generation of energetic electrons and ions [3], and high harmonic generation for nonlinear optics studies [4]. Recently, nuclear fusion of colliding energetic ions from exploding deuterium clusters was also experimentally demonstrated [5].

Experiments on the interaction of an intense laser pulse with cluster gas have demonstrated interesting optical effects such as the self-focusing of the laser pulse [6], strong absorption of the laser pulse energy [7], and spectral broadening of the pulse [8]. In order to understand these effects, we need a model that describes the dynamics of the laser-irradiated cluster as well as the back reaction on the laser pulse. In this paper, we develop a self-consistent model for the propagation of an intense laser pulse in a gas of exploding clusters that acts as a non-linear medium and study the observed experimental effects.

The cluster parameter that directly relates to laser propagation is the individual cluster polarizability γ, defined by the relation $\hat{\mathbf{p}}=\gamma\hat{\mathbf{E}}_L$ where $\mathbf{p}(t)=\mathrm{Re}\{\hat{\mathbf{p}}e^{-i\omega t}\}$ is the electric dipole moment of the cluster and $\mathbf{E}_L(t)=\mathrm{Re}\{\hat{\mathbf{E}}_L e^{-i\omega t}\}$ is the laser electric field whose frequency is ω. The temporal evolution of γ determines the time variation of the effective dielectric constant of the ensemble of clusters given as

$$(\varepsilon_{\mathrm{eff}})_{\mathrm{medium}} = 1 + 4\pi n_c \gamma, \tag{1}$$

where n_c is the number density of clusters. In an experiment on the time-resolved explosion dynamics of laser-irradiated clusters, Kim *et al.* [15] measured the complex cluster polarizability. It is of significance to use an experimentally consistent model of the cluster polarizability γ for any realistic simulation of pulse propagation through cluster plasma.

The earliest cluster models [9,10] described the inner-shell ionization of the cluster atoms, and explained the x-ray emission for small clusters but were unsuitable for the computation of polarizability. One of the first models of cluster expansion that enables the calculation of polarizability was given by Ditmire (see Ref. [11] for details). This model treats the cluster as a spherical ball of uniform density throughout the interaction process. Though this model has been very useful in explaining many aspects of cluster expansion like high ionization levels, generation of energetic ions, and resonant absorption, it has drawbacks in that it predicts strong absorption during time intervals much shorter than those measured in experimental studies [12,13]. Milchberg [14] proposed the fully hydrodynamic model that allows for temperature and density gradients within the cluster. This gives results of cluster dynamics consistent with the experiments measuring the complex transient polarizability of clusters [15]. The polarizability results from the hydrocode are further supported by experiments on scattering and absorption of intense laser pulses in clustered gas [16,17]. This model, however, is computationally intense and thus unsuitable for studies of pulse propagation where effectively many clusters must be simulated. Also, fluid models are not expected to be appropriate at intensities of irradiation that are high enough to create a population of energetic electrons. Alternate to the fluid approach are the kinetic models that treat electrons and ions as particles [18–20]. The particle model can include the effects of energetic particles on the polarizability. However, it is even more computationally intense than the fluid models and the predictions for the cluster polarizability coming from kinetic models have not been fully explored. In addition to these, there are other fluid and kinetic models that aim to explain specific aspects of the laser-cluster interactions such as third harmonic generation [21,22], generation of high charged states of ions [23], self-focusing of the laser pulse [24], and coulomb explosion of very small clusters [25].

We propose a model of cluster expansion that retains the simplifying assumption of a uniform density profile within the cluster, but with modified cluster parameters. Our model

generates a temporal polarizability profile consistent with the hydrodynamic model without sacrificing computational speed. We couple the uniform density model, thus modified, to a Gaussian description of the laser pulse and study the propagation of a laser pulse through a cluster plasma. Our simulation results explain many experimentally observed effects like focusing and strong absorption of the laser pulse. The underlying assumption in our model is that the dominant non-linearity is the intensity dependent rate of expansion of the cluster radius [26]. We assume the electrons respond linearly to the laser field. Energy is absorbed by the cluster due to electron-ion collisions. The heated electrons cause the cluster to expand on a time scale determined by the ion mass. The quasi-linear modification of the cluster profile and radius then changes the linear response of the electrons. Thus we can think of the non-linearity as occurring through the ion motion. This is in contrast to alternative models [21,22,24] that emphasize the direct non-linear response of the electrons in the strong laser fields.

Finally we note that above a threshold intensity the electron motion becomes highly nonlinear and there is strong production of energetic electrons. The model presented here is meant to apply for intensities below this threshold where the electron distribution remains thermal.

In the next section we present in detail the equations and assumptions used for simulating the cluster dynamics. Section III of this paper describes the modeling of the laser pulse and the pulse propagation equations. Equilibrium and stability of the pulse parameters are considered in Sec. IV. The results of numerical simulation are presented in Sec. V.

II. CLUSTER MODEL

Perhaps the most basic model for the heating and expansion of atomic clusters in the presence of intense fields is the uniform density model given by Ditmire *et al.* [11]. In this model, the clusters are treated as uniform dielectric spheres with no temperature or density gradients inside the cluster. The dynamical variables which describe the cluster are the (uniform) electron temperature, electron density and ion density, and radius of the cluster $a(t)$.

If the cluster is much smaller than a laser wavelength, the electric field in and around the cluster can be determined in the electrostatic approximation. Inside the cluster the electric field is uniform and is given by $\mathbf{E}_i(t)=\mathrm{Re}\{\hat{\mathbf{E}}_i e^{-i\omega t}\}$ where

$$\hat{\mathbf{E}}_i = \frac{3}{\varepsilon_{\mathrm{cluster}}+2}\hat{\mathbf{E}}_L, \tag{2}$$

and $\mathbf{E}_L(t)=\mathrm{Re}\{\hat{\mathbf{E}}_L e^{-i\omega t}\}$ is the laser electric field. The dielectric constant inside the cluster, $\varepsilon_{\mathrm{cluster}}$, will be determined mainly by the response of the free electrons and is given by the Drude model [28],

$$\varepsilon_{\mathrm{cluster}} = 1 - \frac{\omega_p^2}{\omega^2(1+i\upsilon/\omega)}, \tag{3}$$

where $\omega_p^2=4\pi n_e e^2/m_e$ is the plasma frequency, e and m_e are the electron charge and mass and υ is the electron-ion collision frequency. For large values of $\varepsilon_{\mathrm{cluster}}$ the electric field is shielded from inside of the cluster, i.e., $|\hat{\mathbf{E}}_i| \ll |\hat{\mathbf{E}}_L|$. An important quantity in determining the evolution of the laser pulse is the response of the cluster to the laser field, which is characterized by the cluster complex polarizability, γ. This is defined by the relation $\hat{\mathbf{p}}=\gamma\hat{\mathbf{E}}_L$ where $\mathbf{p}(t)=\mathrm{Re}\{\hat{\mathbf{p}}e^{-i\omega t}\}$ is the electric dipole moment of the cluster. For a spherical cluster of uniform dielectric constant, $\varepsilon_{\mathrm{cluster}}$, the polarizability of the cluster is

$$\gamma = \frac{\varepsilon_{\mathrm{cluster}}-1}{\varepsilon_{\mathrm{cluster}}+2}a^3, \tag{4}$$

where a is the radius of the cluster.

To apply Eqs. (3) and (4), a model for the evolution of the electron temperature and density in the cluster and the radius of the cluster is required. The free electron density in the cluster evolves due to several processes [14]. Initially free electrons are produced by direct ionization of the cluster atoms in the presence of the laser field. Further ionization occurs via electron-ion inelastic collisions, facilitated by the high density inside the cluster. The free electrons, thus produced, absorb laser-energy primarily through collisional inverse bremsstrahlung process. Finally, the density decreases as the cluster expands. In our version of the model, these processes are treated as follows. We will assume that ionization occurs instantaneously once the intensity exceeds a certain threshold. At that time the cluster atoms will be ionized to a specific state Z. The electron and ion densities are then taken to be $n_e=Z_{n_i}=ZN_a/V$ where N_a is the number of atoms and $V=4\pi a^3/3$ is the volume of the cluster.

The expansion of the cluster is due to the thermal energy of the heated electrons and is restrained by the inertia of the ions. If the cluster remains quasineutral the evolution of the cluster radius can be determined by balancing the rate of increase of ion kinetic energy, $K_i=(2\pi/5)m_i n_i a^3\dot{a}^2$ against the rate at which work is done by the electron pressure in expanding the cluster,

$$\frac{dK_i}{dt} = P_e\frac{dV}{dt} = P_e 4\pi a^2\frac{da}{dt}, \tag{5}$$

where $P_e(t)$ is the electron pressure and m_i is the ion mass. The expansion of the cluster thus obeys

$$\frac{d^2a}{dt^2} = 5\frac{P_e}{m_i n_i a}. \tag{6}$$

The electron pressure is obtained by balancing the rate of increase of internal energy of electrons against the sources and sinks of electron energy,

$$\frac{d}{dt}\left(\frac{3}{2}VP_e\right) = -P_e\frac{dV}{dt} + \dot{U}V, \tag{7}$$

where $\dot{U}$ is the rate of energy absorption per unit volume, given by

$$\dot{U} = \frac{9}{8\pi}\frac{\mathrm{Im}(\varepsilon)}{|\varepsilon+2|^2}\omega|\hat{\mathbf{E}}_L^2|. \tag{8}$$

The model system (5)–(8) is based on the assumption that the density and temperature profiles remain flat within the cluster ($r<a$). This is not true even if one adopts a fluid model. Recent one-dimensional fluid simulations [14] have shown that the density profile develops a low-density pedestal, which has a significant effect on the laser electric field and the rate of energy absorption. Further, if one adopts a kinetic picture it is found that there is generation of energetic electrons that are outside the description of the fluid model [18]. In spite of these shortcomings, the simplicity of the uniform density model makes it attractive for plasma propagation studies, provided it can replicate the dynamic behavior of the cluster polarizability.

To use the model we adjust parameters so that the time dependence of the polarizability matches that of calculations obtained from the fluid code of Ref. [14]. These results for polarizability have also been compared favorably with experimental results [15]. The parameters we adjust are the ion mass and the dependence of the collision frequency on temperature and density. In particular, we assign a mass of 3 atomic units for the ions in the cluster as opposed to the expected 40 amu of normal argon ions. The modified collision frequency is given as

$$\upsilon/\omega = \frac{15}{T_e^{1/4}}, \tag{9}$$

where T_e is the electron temperature in electron volts. The electron temperature is calculated assuming the electrons to behave as an ideal gas with $P_e=n_eT_e$. These two modifications attempt to rectify shortcomings of the uniform density description, as we now describe. From Eq. (4) we note that if $\varepsilon_{\text{cluster}} \gg 1$, then $\gamma \approx a^3$. Thus in the uniform density model the polarizability is real and determined primarily by the cluster radius during the initial expansion. The fluid and the particle simulations show a more complicated picture with the polarizability depending sensitively on the shape of the density profile near the critical surface. In the hydromodel the cluster heating and expansion are primarily determined by the dynamics of the thin critical density layer, as opposed to the uniform density model where the whole cluster comes to resonance at the same time. One could thus argue, that the evolution of the cluster as a uniform dielectric sphere but with reduced mass captures this effect, allowing the cluster to expand more rapidly. This has the effect of allowing the real part of polarizability to increase more rapidly in time, thus giving results comparable to the hydrocode.

Adjusting the temperature and density dependence of the collision rate also affects the imaginary part of the polarizability. If one uses the Spitzer collision rate [29], the uniform density model tends to give an imaginary part of polarizability that is large only during brief times near resonance ($\varepsilon_{\text{cluster}}+2\approx 0$). The fluid simulations, on the other hand, indicate that the absorption occurs for a much larger time period due to the resonance at the critical surface. The modified collision frequency, Eq. (9), allows for this greater absorption. In particular, it provides a greater rate of collisions than the Spitzer formula, and the dependencies on density and temperature are chosen to match the hydrocode results for which the collective rate of absorption is largely independent of the collision frequency.

A comparison of the real and imaginary polarizability using the fluid model and our modified uniform density model is shown in Fig. 1. In each case a 30 nm cluster was irradiated with a laser pulse (100 fs FWHM, 800 nm wavelength) for three different peak intensities 5×10^{14} W/cm^2, 8×10^{14} W/cm^2, and 1×10^{15} W/cm^2. The basic time evolution of the polarizability is the same for both the models. With regards to the optical property of the cluster, the validity of our model has been verified for the range of laser-cluster parameters considered in this work. Our simulations are valid for clusters of initial diameter of the order of a few hundred Angstroms, and laser pulses of intensity 5×10^{14} W/cm^2–1×10^{16} W/cm^2 and pulse width of the order of 100 femtoseconds. These values are very typical of those measured or used in experiments. For parameters outside those considered here it is likely that modifications to the model would be necessary. The agreement between the two models starts failing as the density within the cluster falls below the critical density, i.e., as the cluster disassembles. However, except for very long pulse-widths, this happens after the laser pulse has passed over the cluster and so is not important from the point of view of pulse propagation and self-guiding.

Clusters at different radial distances from the axis of propagation of the pulse will experience different temporal profiles of laser intensity due to the variation of intensity with radius. This will lead to a spatially and temporally varying effective dielectric constant through the variations of polarizability. Figure 2 shows a contour plot, in the $r-\xi$ plane, of the real (a) and imaginary (b) polarizability for 30 nm clusters irradiated by laser pulse (800 nm, 100 fs FWHM, 40 μm radial FWHM, 1×10^{15} W/cm^2). After the clusters are ionized, the polarizability decreases with increasing radial distance in the region of rising Re(γ). Parts of the pulse that propagate through this region will be focused. After Re(γ) peaks and starts decreasing this trend reverses. The temporal variation in polarizability is also responsible for frequency shifts in the pulse spectrum. Specifically, rising Re(γ) will lead to redshifts in the spectrum while decreasing Re(γ) will cause the spectrum to blueshift. As seen in (b) the Im(γ) rises in magnitude only at a later time within the pulse. This should lead to a preferential strong absorption of the pulse tail. These effects are discussed in details when we present the results of numerical simulations of pulse propagation.

III. LASER PULSE PROPAGATION

In this section we review the derivation of the laser envelope equations and discuss how these equations are combined with the cluster evolution equations of the previous section. We assume that the cluster gas is tenuous, having a

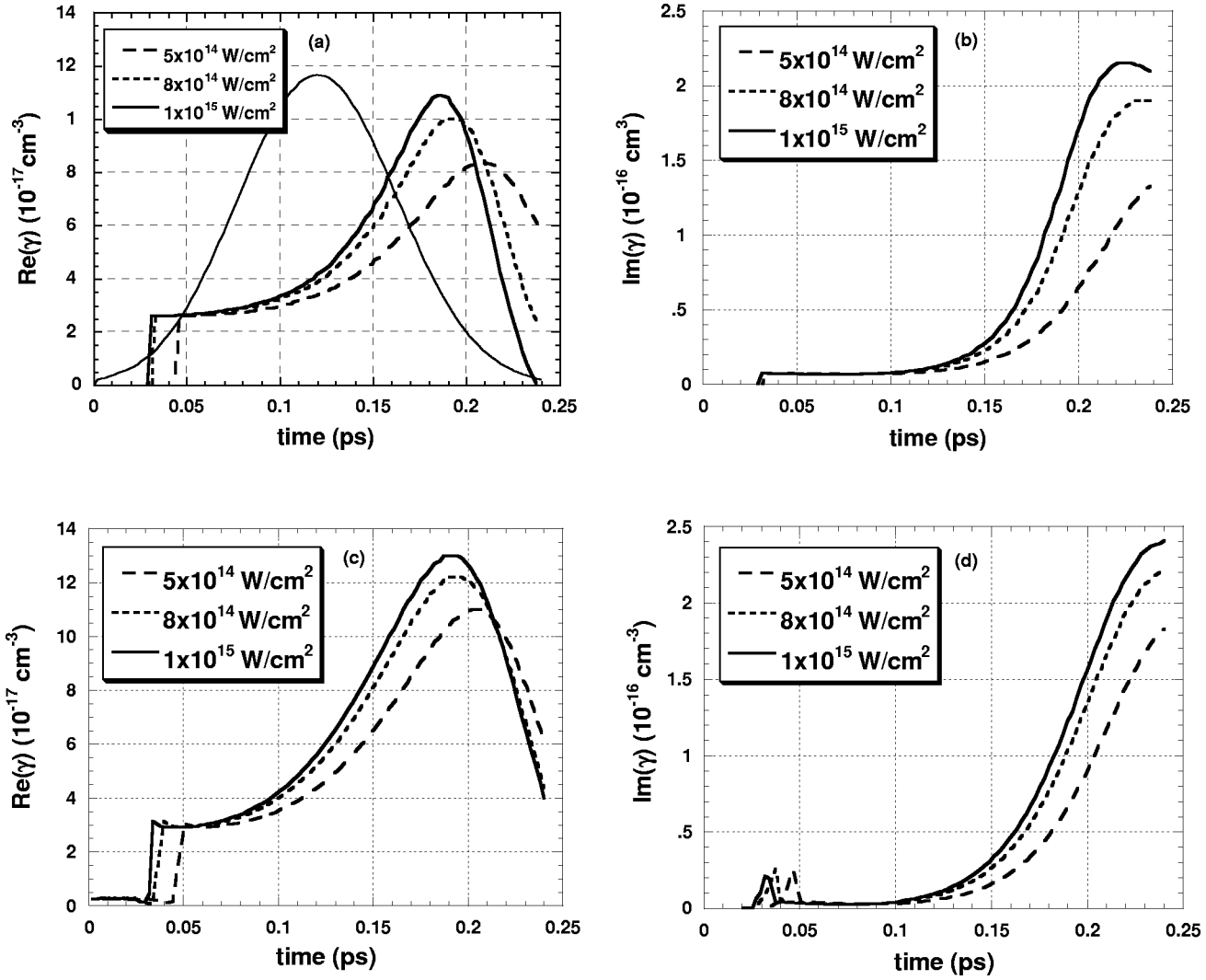

FIG. 1. A comparison of the real and imaginary polarizability for our model (a),(b) and the hydrocode of Milchberg (c),(d). In each case, a cluster of initial radius 30 nm is irradiated with an 800 nm, 100 fs FWHM laser pulse for three different peak intensities 5×10^{14} W/cm^2 (dashed), 8×10^{14} W/cm^2 (dotted), and 1×10^{15} W/cm^2 (solid, dark). The pulse profile is shown in (a) as a thin solid line.

small effective dielectric constant. In this case the laser pulse will evolve slowly as it propagates at nearly the speed of light. The laser field is then represented by a complex amplitude $\mathbf{E}_L(\mathbf{x}_\perp,z,t)=\mathrm{Re}\{\hat{\mathbf{E}}_L(x_\perp,\xi,z)e^{-i\omega\xi}\}$, where $\xi=t\text{-}z/c$ is a time variable in the laser frame. The effective dielectric constant is given by

$$\varepsilon = 1 + \delta\varepsilon(\mathbf{x}_\perp,\xi,z) = 1 + 4\pi n_c \gamma, \tag{10}$$

where n_c is the density of clusters, and $\gamma(\mathbf{x}_\perp,\xi,z)$ is the local average polarizability of clusters at the point $(\mathbf{x}_\perp,z)$ and depends on time through the variable ξ. By average, we imagine that there are many clusters in a small volume whose size is small compared to the distance over which the laser envelope varies. In doing so we neglect Rayleigh scattering due to discreteness of the clusters. Finally, while cluster gases typically contain a distribution of cluster sizes, we will assume for the present that the average polarizability can be computed based on a single initial cluster size.

Applying the slowly varying envelope approximation, we can express the evolution of the envelope in terms of the variables $\mathbf{x}_\perp$, z, $\xi=t-z/c$, as

$$\left(\nabla_\perp^2 + k_0^2\delta\varepsilon_{\mathrm{eff}} + 2ik_0\frac{\partial}{\partial z}\right)\hat{\mathbf{E}}_L = \mathbf{0}, \tag{11}$$

where $k_0=\omega/c$. It is important to note that while Eq. (11) contains only a z derivative, the amplitude $\hat{\mathbf{E}}_L$ and the effective dielectric constant $\delta\varepsilon_{\mathrm{eff}}$ both depend on time (ξ) in addition to z. The time variation of $\delta\varepsilon_{\mathrm{eff}}$ is obtained by integrating the cluster expansion equations with t replaced by ξ.

Considering that clusters at different transverse locations experience different laser intensities, the combined system of equations is complicated. As a first step, in this paper, we will solve Eq. (11) using the source-dependent expansion technique, following Ref. [27], in which the field envelope is expressed in terms of a series of Laguerre-Gaussian functions as

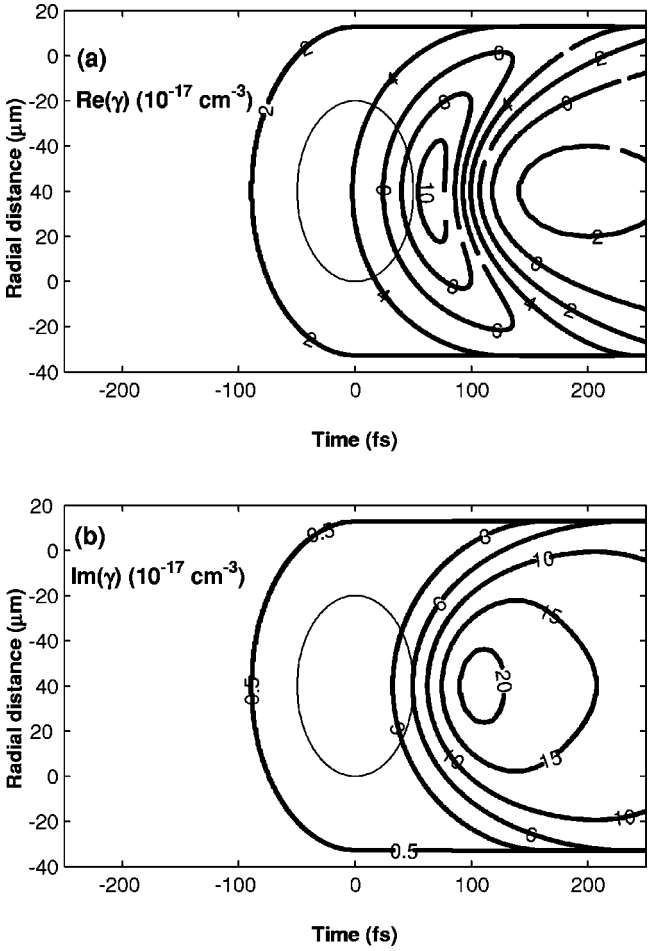

FIG. 2. Contour plot of (a) real and (b) imaginary part of polarizability. The ellipse in the center of each plot marks FWHM points.

$$\hat{\mathbf{E}}_L = \sum_{m=0,1,2\ldots} \hat{\mathbf{E}}_m L_m(X) e^{-(1-i\alpha)X/2}, \tag{12}$$

where $\hat{\mathbf{E}}_m(\xi,z)$ is the complex amplitude, $L_m(X)$ is the Laguerre polynomial, $X=2r^2/R^2$, $R(\xi,z)$ is the spot size, and $\alpha(\xi,z)$ is related to the curvature of the wave fronts. The expression for the field envelope is then substituted in Eq. (11) and truncated at the lowest order Gaussian mode assuming that the higher order modes are small and can be neglected. Extending the equations derived in Ref. [27] for the lowest order mode to the case of a complex dielectric constant, and putting $\hat{\mathbf{E}}_0=\mathbf{E}_s e^{i\theta}$ we obtain the following equations to describe the parameters in Eq. (12):

$$\frac{\partial E_s}{\partial z} = -E_s\left(\frac{2}{k_0}\frac{\alpha}{R^2} + H_i + G_i\right), \tag{13}$$

$$\frac{\partial \theta}{\partial z} = -\frac{2}{k_0}\frac{1}{R^2} + H_r + G_r, \tag{14}$$

$$\frac{\partial R}{\partial z} = \frac{2}{k_0}\frac{\alpha}{R} + RH_i, \tag{15}$$

and

$$\frac{\partial \alpha}{\partial z} = \frac{2}{k_0}\frac{1+\alpha^2}{R^2} - 2(H_r - \alpha H_i), \tag{16}$$

where

$$G_{r,i} = \frac{k_0}{2}\int_0^\infty dX(\delta\varepsilon_{r,i}e^{-X}) \tag{17}$$

and

$$H_{r,i} = \frac{k_0}{2}\int_0^\infty dX(\delta\varepsilon_{r,i}(1-X)e^{-X}). \tag{18}$$

Here $\delta\varepsilon_r$ and $\delta\varepsilon_i$ are the real and imaginary parts of $\delta\varepsilon_{\text{eff}}$, the change in dielectric constant determined by the cluster response. Equation (13) describes the evolution of the field amplitude. The first term on the right describes the effect of diffraction while the second and third describes the effect of absorption. Equation (14) describes the evolution of the laser phase, $\theta(\xi,z)$. The ξ dependence of the phase gives the frequency shift on axis. Here time variations of the polarizability will contribute to the H_r and G_r terms and give frequency shifts. Equations (15) and (16) describe the evolution of the spot-size $R(\xi,z)$ and the phase front curvature $\alpha(\xi,z)$, with the first term in each equation describing the effect of diffraction. In addition to the diffractive terms, the radial dependence of the $\delta\varepsilon_{\text{eff}}$ will contribute to focusing and defocusing of the laser pulse. If $\delta\varepsilon_r$ and $\delta\varepsilon_i$ are peaked on axis then both H_r and H_i will be positive. The usual focusing effect due to an on-axis peak on $\delta\varepsilon_r$ is manifested by the H_r term in Eq. (16). A positive value of H_r causes the phase front curvature to become negative and leads to focusing through Eq. (15). There are additional defocusing effects associated with H_i. A positive H_i will cause defocusing in Eq. (15) due to preferential absorption of energy at small r and also leads to an increase in the curvature of the wave front.

We emphasize that the parameters E_s, θ, R, and α are functions of both axial distance z and laser frame time coordinate $\xi=t-z/c$. Equations (13)–(16) govern the evolution of these parameters in z with ξ being present as a parameter. The evolution of the laser pulse at different ξ values is coupled through equations determining the time dependent dielectric constant $\delta\varepsilon_{\text{eff}}(r,\xi,z)$. Basically, these are Eqs. (6)–(8) with the time derivative replaced according to $\partial/\partial t \rightarrow \partial/\partial\xi$. The heating rate in Eq. (8) depends on the intensity of the laser pulse, which has a Gaussian radial profile with a time and space varying amplitude and spot size. Solutions of this coupled system of equations will be explored in the subsequent sections.

IV. EQUILIBRIUM AND STABILITY OF THE SELF-GUIDED SOLUTION

The focusing properties of the cluster plasma are described by the time dependent functions H_r and H_i defined by Eq. (18). These functions are proportional to the cluster density n_c and the time dependent polarizability γ. The polarizability depends on the properties of the laser pulse through the heating rate in Eq. (8).

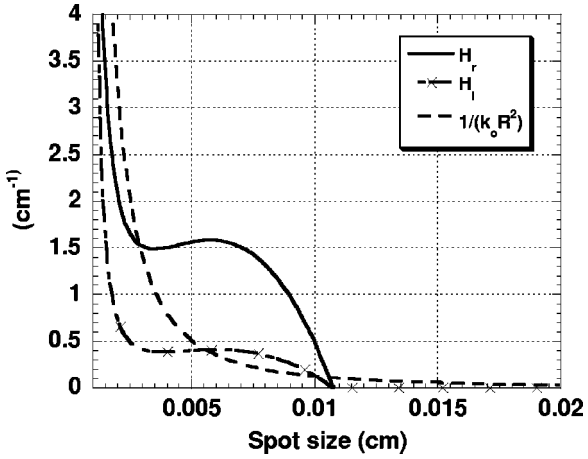

FIG. 3. The quantities $H_r(\xi=0$ fs) (solid) and $H_i(\xi=0$ fs) (dashed with cross markers) are plotted at $z=0.006$ cm. Here the cluster density set to $n_c=3\times10^{11}$ cm^{-3} and the spot size of the pulse was varied from 10 μm to 200 μm. All other parameters were initialized to the conditions in Table I. The intersection of H_r with the $1/k_0R_0^2$ curve (dashed) gives the equilibrium values of R for the chosen cluster density.

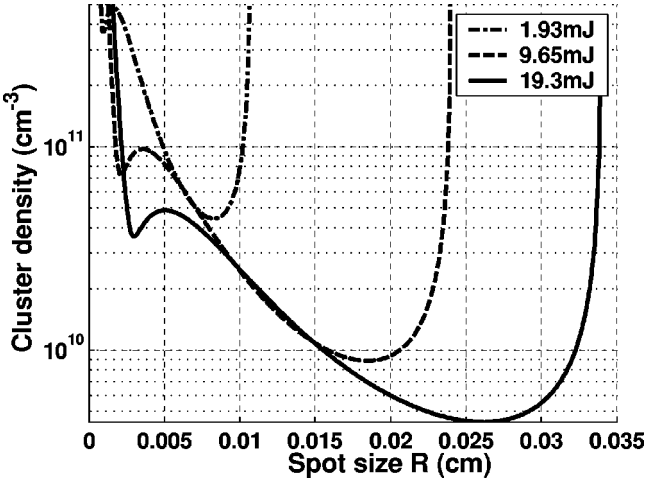

FIG. 4. Cluster density required for equilibrium of a pulse as a function of the pulse spot size for three different initial energies 1.93 mJ (dash-dot), 9.65 mJ (dashed), and 19.3 mJ (solid). All other parameters were initialized to the conditions in Table I. Note that for a pulse with given initial energy the same cluster density can occur for two values of R.

We first consider the behavior of H_r and H_i when the laser pulse is specified to have a given energy, duration and spot size. Specifically we consider the case of a 100 fs FWHM Gaussian envelope pulse centered at $\xi=0$ as in Fig. 1(a). The time dependence of the polarizability leads to time dependent values of H_r and H_i. Accordingly, through Eqs. (13)–(16) the pulse parameters E_s, θ, R, α will evolve in a time dependent way. Solutions of this process will be presented in the next section. Here we consider the values of H_r and H_i that are obtained at $\xi=0$ fs corresponding to the peak of the injected pulse. The dependence of these quantities on spot size and laser power will give insight into the guiding mechanism that occurs in cluster plasma. The values of the functions H_r and H_i are determined by first assuming that the radiation field has the following form, consistent with Eq. (12) truncated at one term,

$$\mathbf{E}_L(\xi,r,z)=\mathbf{E_s}(\xi,z)e^{i\theta(\xi,z)-(1-i\alpha(\xi,z))r^2/R^2(\xi,z)}, \qquad (19)$$

where for the moment we assume α and R are constants. We then solve Eqs. (6)–(8) on a grid in r and compute the r and ξ dependent complex polarizability γ from Eq. (4). A sample of this is shown in Fig. 2. The perturbed complex dielectric constant $\delta\varepsilon=4\pi n_c\gamma$ is inserted in Eqs. (17) and (18), which are then numerically integrated in r to obtain $H_{r,i}$ and $G_{r,i}$.

We now consider the focusing of the pulse, which is determined primarily by H_r and H_i through Eqs. (15) and (16). Figure 3 shows plots of H_r and H_i at $\xi=0$ fs versus the spot size R for a pulse of fixed energy (1.92 mJ) and assuming $n_c=3\times10^{11}$ cm^{-3}. The dependence of these curves on radius will determine the equilibrium and stability of guided states.

We first look for the equilibria by demanding $\partial R/\partial z=0$ and $\partial\alpha/\partial z=0$ in Eqs. (15) and (16). According to Eq. (15), in equilibrium $\alpha=-k_0R^2H_i/2$, that is, the phase fronts are slightly curved inwards. However, for the values of H_i indicated in Fig. 3 and for the value $k_0=2\pi/\lambda=7.85\times10^4$ cm^{-1} we find that $\alpha\ll1$. Thus we further simplify our analysis by neglecting H_i and taking the equilibrium to be $\alpha=0$, and $R=R_0$ where from Eq. (16) $H_r(R_0)=1/k_0R^2$. The quantity $(1/k_0R^2)$ is also plotted on Fig. 3 and we note that there are two possible equilibrium values where the H_r and $(1/k_0R^2)$ curves intersect ($R=28$ μm and $R=130$ μm). We will show later that only one of these values is stable.

An alternate way of specifying the equilibrium conditions is to note that H_r is proportional to the cluster density n_c. Thus, for any spot size R, we can adjust n_c until the equilibrium conditions are satisfied. This is shown in Fig. 4 where the cluster density that will maintain the spot size at a fixed value is plotted for several values of pulse energy. It can be seen that for a given pulse energy there is a minimum cluster density required to have self-guided equilibria. In particular, for the case of pulse with energy 1.93 mJ (corresponding to a peak intensity of 1×10^{15} W/cm^2 for the pulse parameters of Tab1e I), this minimum cluster density is 4.2×10^{10} cm^{-3}. Also, for a given density there may be two or three equilibrium spot sizes.

We now study the stability of small perturbations away from the equilibrium for our simplified system. We consider the phase front curvature and spot size to be given by $\alpha=\delta\alpha(z)$ and $R=R_0+\delta R(z)$ where R_0 is the equilibrium spot size. Linearizing Eqs. (15) and (16) yields

$$\frac{\partial(\delta R)}{\partial z}=\frac{2}{k_0}\frac{\delta\alpha}{R_0}, \qquad (20)$$

$$\frac{\partial(\delta\alpha)}{\partial z}=-\left(\frac{4}{k_0R_0^3}+2\left.\frac{\partial H_r}{\partial R}\right|_{R=R_0}\right)\delta R. \qquad (21)$$

Note, we have again neglected H_i assuming $\alpha\ll1$. We look for exponential solutions of the form $\delta\alpha$ and $\delta R\sim\exp(\kappa z)$, and find

TABLE I. Initial conditions for numerical simulation of laser pulse propagation through clustered gas.

Pulse	Cluster
Wavelength =800 nm	Initial radius =30 nm
Pulse width =100 fs FWHM	Threshold intensity
Peak Intensity $=1\times10^{15}$ W/cm^2	for ionization $=1\times10^{14}$ W/cm^2
Spot size = 40 μm FWHM	Degree of ionization =9
Phase(θ)=0	Ion density $=1.8\times10^{22}$ cm^{-3} $=10n_{critical}$
Curvature (α)=−.1284 (determined by equilibrium conditions at $\xi=0$)	Cluster density $=2.19\times10^{11}$ cm^{-2}
Energy=1.93 mJ	(determined by equilibrium conditions at $\xi=0$)

$$K^2 = -\frac{4}{K_0 R_0^4}\left[2 + \left(\frac{R}{H_r}\frac{\partial H_r}{\partial R}\right)\Bigg|_{R=R_0}\right]. \quad (22)$$

Thus the requirement for stability of an equilibrium is

$$\left(2H_r + R\frac{\partial H_r}{\partial R}\right)\Bigg|_{R=R_0} > 0, \quad (23)$$

where we note that $H_r > 0$ is required for equilibrium. Note also that this condition does not depend on the cluster density, only the spot size, pulse energy and pulse duration matter.

The left-hand side of Eq. (23) is plotted vs R_0 for several pulse energies in Fig. 5. We see that in the 1.93 mJ case equilibria are unstable for $10\ \mu\text{m} < R < 14\ \mu\text{m}$ and $R > 82\ \mu$m. Thus the 130 μm equilibrium spot size found in the $n_c = 3\times10^{11}$ cm^{-3} case is unstable, while the $R_0 = 28\ \mu$m case is stable according to the simple model.

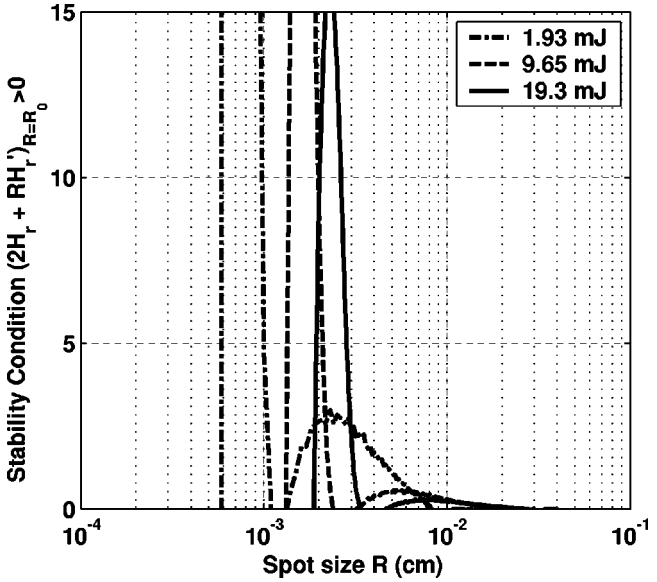

FIG. 5. Stability expression $(2H_r + R\partial H_r/\partial R)_{R=R0}$ vs spot size R for a laser beam for three different initial pulse energies 1.93 mJ (dash-dot), 9.65 mJ (dashed), and 1.93 mJ (solid) All other parameters initialized to the conditions in Table I. The range of R over which the plotted quantity is positive is stable. For example, in the 1.93 mJ case, the region of stability corresponds to 14 μm $< R <$ 82 μm and $R <$ 8 μm.

V. NUMERICAL SIMULATIONS RESULTS

In this section we present the numerical simulation results for the propagation of laser pulses through a clustered gas based on the coupled Eqs. (6), (7), and (13)–(18). For the following numerical simulation results, the initial parameter values for the cluster and the laser field are given in Table I. These parameters are similar to those typically seen in the laboratory. Unless otherwise mentioned the results refer to quantities at $\xi=0$, the center of the laser pulse.

Contrary to the low energy absorption when a tenuous gas is irradiated by laser, clustered gases absorb laser energy very efficiently. This has an important impact on the applications of the laser-cluster interaction process like x-ray production and generation of energetic particles. Figure 6 shows the power within the pulse for different distances of propagation. The laser-cluster system was initialized to the values in Table I. As seen in the figure, the power is quickly absorbed at the tail end of the pulse, while the front remains unattenuated. Absorption of pulse energy is due to the positive imaginary part of the complex cluster polarizability. The strong absorption of laser energy at latter times in the pulse is a consequence of the sharp rise in Im(γ) at those times (see Fig. 2). The front of the pulse, where the intensity is below the critical intensity for ionization of the cluster, propagates through unionized clusters and is not absorbed.

Figure 7 shows the evolution in energy and spot size of the pulse with propagation distance z, for the initial conditions in Table I. We note that by 1.5 cm the pulse has depos-

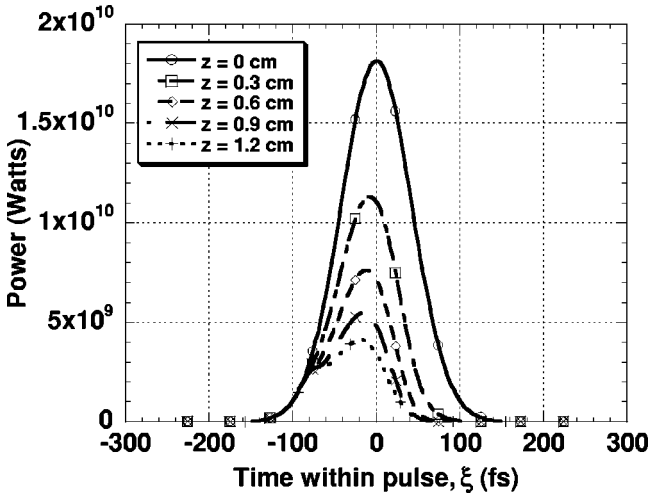

FIG. 6. Power within the pulse (initial parameters of Table I) at $z=0$ cm, 0.3 cm, 0.6 cm, 0.9 cm, and 1.2 cm. The front of the pulse, traveling through unionized clusters, does not get absorbed and hence propagates unattenuated while the trail end (where the imaginary part of polarizability is high) is strongly attenuated.

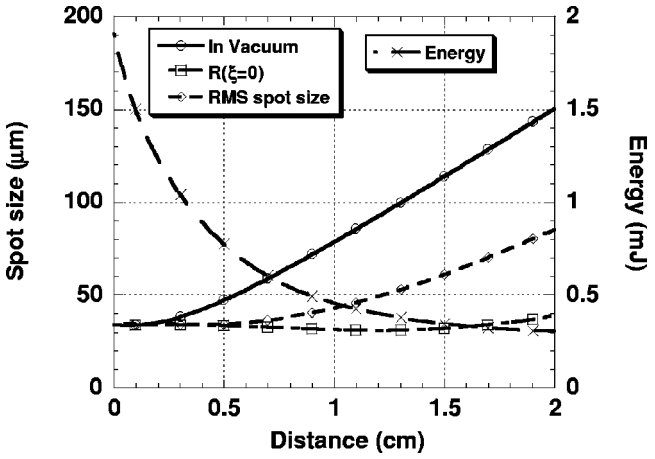

FIG. 7. Self-guiding of the laser pulse in cluster medium. The figure shows the spot size at the center of the pulse ($\xi=0$ fs) (dashed with square marker) for propagation through 2.0 cm of clustered gas for the initial conditions of Table I. The result for propagation through vacuum (solid with circle markers) is plotted for comparison. The rms (root mean squared) spot size is also shown (dashed with diamond markers). The center of the pulse remains focused for roughly 1.5 cm. The energy within the pulse (solid with cross markers) is plotted in mJ (right axis). We note that about 83% of the pulse energy is absorbed by the clusters in 1.5 cm of propagation, after which the rate of absorption levels off.

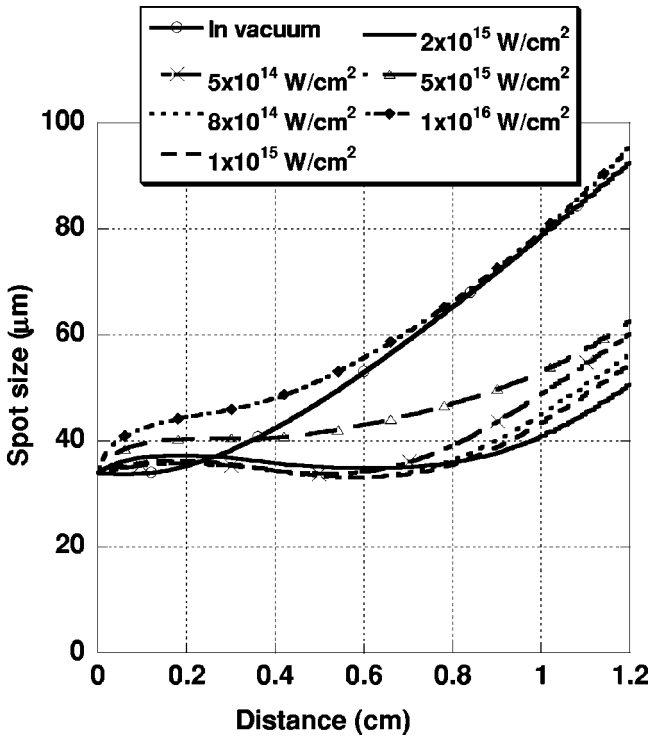

FIG. 8. rms spot sizes as a function of propagation distance for pulses with six different initial peak intensities: 5×10^{14} W/cm^2, 8×10^{14} W/cm^2, 1×10^{15} W/cm^2, 2×10^{15} W/cm^2, 5×10^{15} W/cm^2, and 1×10^{16} W/cm^2. Here cluster density was set to $n_c=3\times10^{11}$ cm^{-3}, other initial conditions being those in Table I. We note that the guiding effect is strongest around peak intensity of 2×10^{15} W/cm^2. The evolution of spot size for a pulse propagating in vacuum is plotted for comparison.

ited 83% of its energy in the gas. After this the pulse energy changes little. Two measures of the spot size are plotted: the instantaneous spot size at $\xi=0$ and the rms spot size weighted by the time-dependent pulse power. The spot size for propagation through vacuum is plotted for comparison and to illustrate the guiding effect. Both the instantaneous and RMS spot sizes expand less in clustered gas medium than in vacuum. The effective Rayleigh length in this case is seen to be $\sim$1.2 cm while that in vacuum is 0.45 cm. The center of the pulse however, as seen via $R(\xi=0\text{ fs},z)$ remains distinctly focused for more than 1.5 cm. Such self-focusing has been experimentally observed by Kim *et al.* [15] where they focus 7.5 mJ, 800 nm pulses with pulsewidths in the range 80 fs$-$1.4 ps into clustered argon.

Next we try to explore the effect of initial energy on the focusing property of the interaction for a fixed pulse width. A comparison of the laser beam RMS spot size is plotted in Fig. 8 for the different initial energies. For this simulation, pulses of different initial energy (set by varying the peak initial intensity) were propagated through clustered gas having the initial laser-cluster parameters as in Table I but the cluster density was set to 3×10^{11} cm^{-3} and the initial curvature was set to zero. It is seen, for such a configuration, that we achieve optimal guiding for intensities around 2×10^{15} W/cm^2. For lower energies, the pulse intensity falls below the threshold value very soon causing the pulse to diffract in the medium of unionized clusters. For higher peak intensities, a larger temporal portion of the pulse faces a defocusing profile of Re(γ), as seen in Fig. 1, causing the rms spot size to be larger.

A comparison of the energy absorbed versus propagation distance is plotted for each of these cases in Fig. 9. We note that the rate of absorption of laser energy increases as we increase the initial energy. Higher peak intensity results in a larger value of the imaginary part of polarizability γ leading to a higher value of H_i and G_i. These directly lead to an increased attenuation rate for the laser field amplitude (and thus energy) via Eq. (13). Moreover, greater peak intensity causes clusters to ionize and thus absorb laser energy over a larger radial zone. As the pulse advances, however, a reduced intensity laser field has lesser potential for ionization and further absorption. Thus the rate of energy absorption tapers off.

As the pulse propagates, different parts of the pulse experience different dielectric constants, due to the time dependence of the cluster polarizability γ. Thus the pulse picks up a time-dependent phase leading to local frequency shift or chirp, $\Delta\omega$. This is given by

$$\Delta\omega = -\frac{\partial\theta}{\partial t} \tag{24}$$

and represents the frequency shifts on axis ($r=0$). Figures 10(a) and 10(b), respectively, show the variation in the on axis phase and the chirp within the pulse, at different distances of propagation. Around $\xi=-80$ fs, the phase shows a

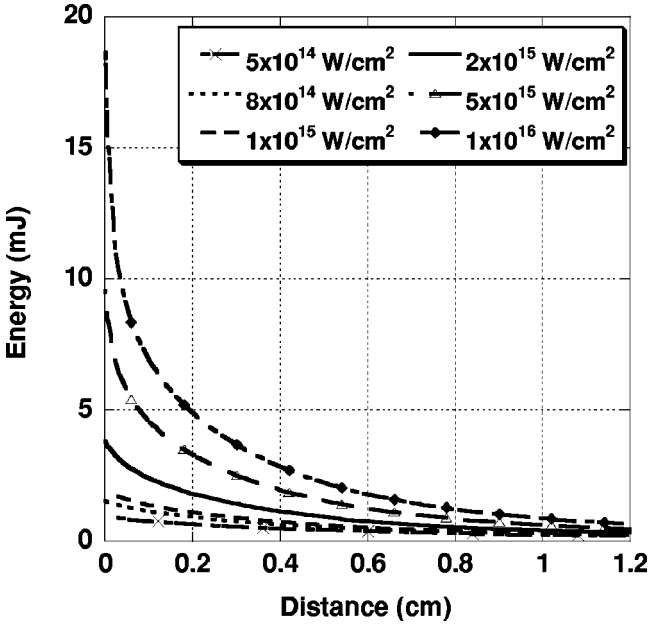

FIG. 9. Variation of energy within the pulse with propagation for pulses of different initial peak intensities: 5×10^{14} W/cm^2, 8×10^{14} W/cm^2, 1×10^{15} W/cm^2, 2×10^{15} W/cm^2, 5×10^{15} W/cm^2, and 1×10^{16} W/cm^2. Here cluster density was set to $n_c=3\times10^{11}$ cm^{-3}, other initial conditions being those in Tab1e I. Pulses with higher initial energy have a higher rate of energy absorption initially. As the pulse energy gets depleted the rate of absorption falls.

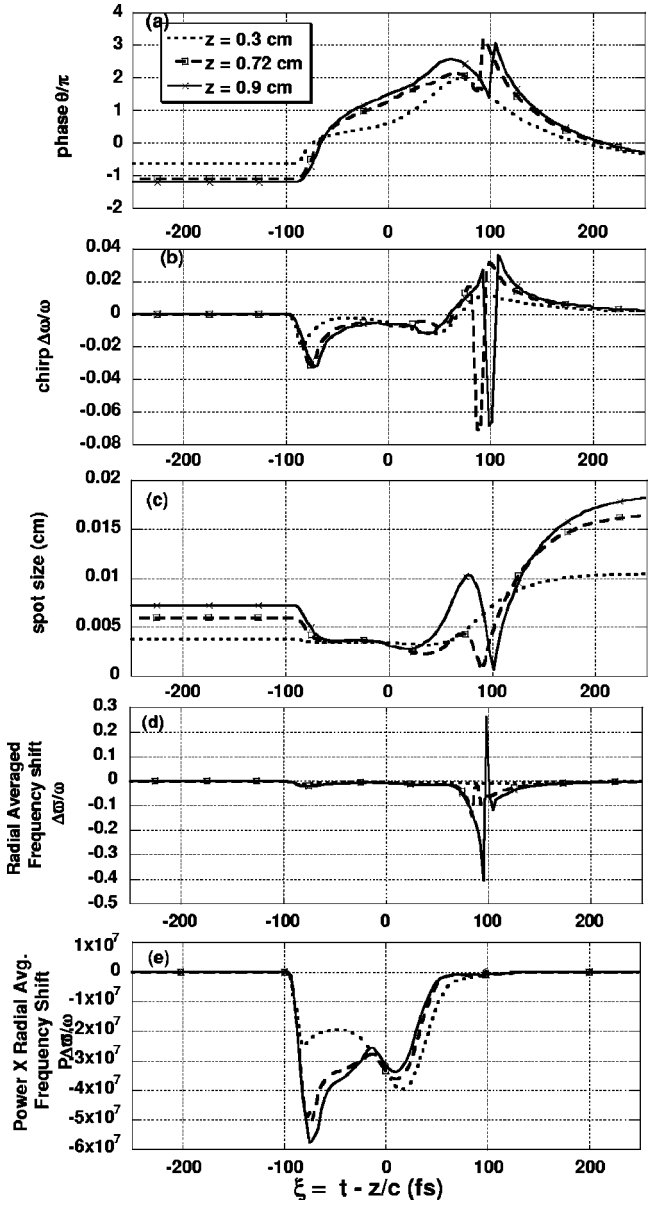

FIG. 10. (a) Phase, (b) chirp developed, (c) spot size of the pulse, (d) radially averaged frequency shift, and (e) power weighted radial averaged frequency shift, at $z=0.3$ cm, $z=0.72$ cm, and 0.9 cm (for initial conditions of Table I). The rise in phase at $\xi=-80$ fs is due to ionization and appears in (b) and (d) as a redshift. The $z=0.72$ cm curve shows a kink in phase at around $\xi=86$ fs. This is due to the sharp focusing of the pulse as seen in (c) and provides further redshift as seen in (b) and (d). The frequency shift weighted with power gives the effect of the propagation on the pulse spectrum.

sudden rise, leading to a red shift as seen in the chirp. At this time, the intensity of the pulse exceeds the threshold intensity causing ionization and a positive jump in the polarizability that appears as a frequency redshift. At $z=0.72$ cm there is a sudden kink in phase for $\xi=86$ fs. This is reflected in the chirp as a strong red shift. The position of this kink moves towards increasing ξ with z. Also, as seen in Fig. 10(c) the spot size R shows a sharp focusing at the same position where the kink occurs in phase. This time dependent focusing in the pulse gives rise to the kink in phase and the associated redshift.

To understand this focusing we examine the governing equations more closely. From Eq. (14) we see that the evolution of the phase is governed by three terms—the first term, which is the diffraction term, and contributions due to the real polarizability, the H_r, and G_r terms. Since all the three terms are functions of spot size R, the variation in R is significant in understanding the behavior of the phase. Figure 11 shows the evolution of the (a) spot size (R), (b) curvature (α), and (c) phase (θ) for two different ξ values ($\xi=86$ fs and $\xi=101$ fs) around the region where the kink occurs in phase. The curve corresponding to $\xi=0$ fs is provided for comparison. The initial pulse parameters were selected so that the $\xi=0$ fs portion of the pulse is in equilibrium and as seen in Fig. 11 the spot size and curvature at $\xi=0$ remain relatively constant. Other parts of the pulse do not start in an equilibrium state and the spot size and curvature vary with distance. Let us consider these nonequilibrium curves. Initially both H_r and H_i are positive while the phase front curvature α is close to zero. Consequently, the spot size R will increase according to Eq. (15) and α decreases because the focusing term $2H_r$ in Eq. (16) is larger than the diffractive term, $2/(k_0R^2)$. As the phase front curvature becomes more negative the rate of increase in spot size decreases and eventually the spot size begins to decrease. That is, the pulse begins to focus. As the spot size decreases, the diffraction term in Eq. (16) becomes more important and the phase front

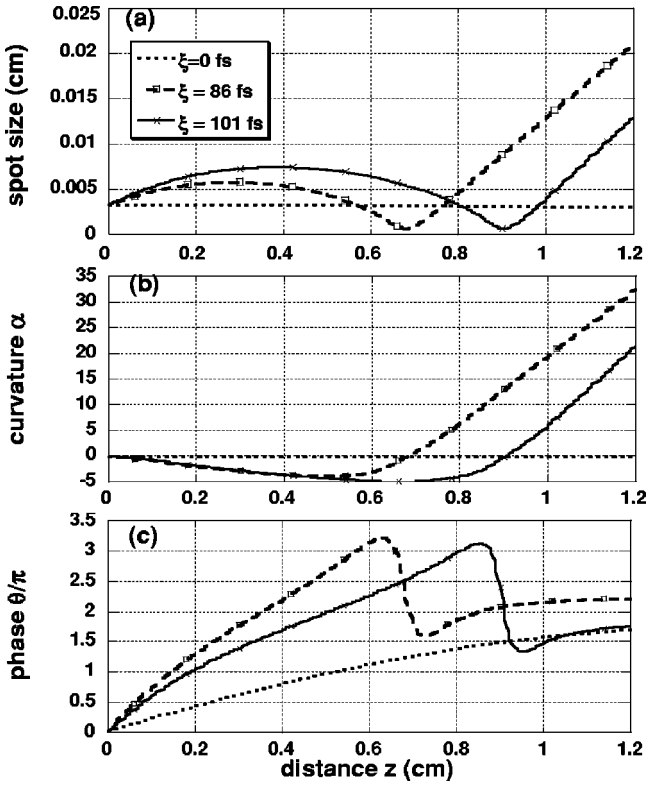

FIG. 11. Variation with propagation distance of spot size (a), curvature (b), and phase (c) of the pulse at three different locations within the pulse ($\xi=0$ fs, 86 fs, 101 fs). The moving focus seen in (a) causes a sharp fall in phase (c).

curvature α begins to increase. At the focal point, where the spot size attains its minimum value the curvature is approximately zero. After the focal point the curvature and spot size increase as in simple diffraction. As the spot size R passes through its minimum value at the focal point there is an abrupt decrease in phase due to the first term in Eq. (14). This decrease in phase occurs earlier for the portion of the pulse at $\xi=86$ fs than for the portion of the pulse at $\xi=101$ fs, as is shown in Fig. 11(c). Consequently, the phase as a function of ξ at fixed z shows a sharp increase at the ξ location separating portions of the pulse that have already focused from those which are yet to focus.

The on-axis frequency shift $\Delta\omega=\partial\theta/\partial\xi$ describes the change in the frequency components at $r=0$. In the previous example we have seen that the phase aquires a time dependence because of the moving focus and the diffractive term, $-2/(k_0R^2)$ in Eq. (14). The abrupt change in phase that occurs as a portion of the pulse passes through a minimum in spotsize is a linear effect. The same term is responsible for the Guoy phase shift that occurs when a Gaussian beam is focused. The pulse's frequency components are actually changed due to the time dependence of the phase, the spot size, and the phase front curvature that occurs due to the time dependent medium. These different spectral components then arrive at the axis at different times giving rise to the abrupt change in the on-axis phase. A quantity which is indicative of the radially averaged frequency is

$$\Delta\varpi(\xi,z) = -\,\mathrm{Im}\left\{\int_0^\infty 2\pi r\,dr\mathbf{E}^*\,\partial\mathbf{E}/\partial\xi\right\}\Big/\int_0^\infty (2\pi r\,dr|\mathbf{E}|^2). \tag{25}$$

Using Eq. (19) we find this to be given by

$$\Delta\varpi = -\left(\frac{\partial\theta}{\partial\xi}+\frac{R^2}{2}\frac{\partial}{\partial\xi}\left(\frac{\alpha}{R^2}\right)\right). \tag{26}$$

According to Eqs. (14)–(16) this quantity satisfies

$$\frac{\partial}{\partial z}\Delta\varpi(\xi,z) = -\left(\frac{\partial G_r}{\partial\xi}+\frac{2H_r}{R}\frac{\partial R}{\partial\xi}\right)-H_iR^2\frac{\partial}{\partial\xi}\left(\frac{\alpha}{R^2}\right). \tag{27}$$

The first term on the right side of Eq. (27) describes the effect if the changing real part of the dielectric constant on the frequency. We note from Eqs. (17) and (18) that

$$\left(\frac{\partial G_r}{\partial\xi}+\frac{2H_r}{R}\frac{\partial R}{\partial\xi}\right)=\frac{k_o}{2}\int_0^\infty dX\left(\frac{\partial\delta\varepsilon_r}{\partial\xi}\right)e^{-X}. \tag{28}$$

The second term on the right represents the effect of radial variations in the absorption on the radially averaged frequency shift. A plot of $\Delta\varpi(\xi,z)$ vs ξ for different distances of propagation is shown in Fig. 10(d) for a laser-cluster system initialized to conditions in Table I. A redshift in frequency occurs at the time when the cluster ionizes. Also, the figure indicates a strong red shift at times when the kink occurs in phase. However, we should note that a high negative (positive) value of the radial averaged frequency shift will not translate to a strong red (blue) shift in the pulse spectrum if the power at that location is very small. Thus a better measure of the effect on the pulse spectrum would be given by the radial averaged frequency shift weighted by the power. This is plotted in Fig. 10(e). It indicates strong redshift at time of ionization of clusters and due to the time-dependent dielectric constant. This should lead the pulse spectrum to be redshifted. For our pulse of 100 fs FWHM, there is very little power at the location in the pulse where the kink occurs. Thus this abrupt change in phase does not have a strong effect on the pulse spectrum. However, this effect may become important for pulses of longer duration. This is yet to be explored.

The pulse spectrum at different distances of propagation, $z=0$ cm, 0.3 cm, 0.6 cm, 0.9 cm, and 1.2 cm, is plotted in Fig. 12. As the pulse propagates it spreads in frequency due to the temporal behavior of $\mathrm{Re}(\gamma)$. A rising $\mathrm{Re}(\gamma)$ causes a redshift while decreasing $\mathrm{Re}(\gamma)$ causes the pulse spectrum to have a blue shift. Additional redshift occurs due to the development of the moving focus described above. Such spectral broadening is also consistent with recently reported experimental results [8].

VI. CONCLUSION

We have described a self-consistent model for the simulation of laser pulse propagation through a gas of exploding

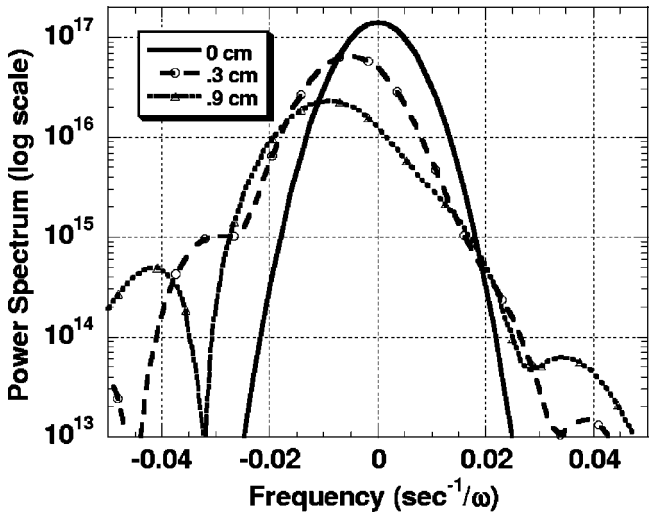

FIG. 12. Power spectrum of the pulse (in logarithmic scale) for $z=0$ cm, 0.3 cm, and 0.9 cm. We see the spectrum broadening with propagation and significant redshifting of the initial spectrum.

clusters. Stability and equilibrium of the system are also studied. We find that for typical laser cluster parameters there are multiple equilibria but not all of them will be stable. For our particular case, we found two sets of parameters that support equilibria but only one was found to be stable. Also, there is a minimum required cluster density for equilibrium of a pulse with fixed energy. For example, in our case of 1.93 mJ pulse, this minimum cluster density was 4.2×10^{10} cm^{-3}.

Our simulations indicate that starting from an equilibrium value the laser pulse typically remains focused for distances of the order of 1.5 cm. The focusing length, however, varies with the pulse peak intensity (other parameters remaining constant), and for the system considered we obtained the maximum focusing distance for a pulse of peak intensity 2×10^{15} W/cm^2. There is very efficient coupling of the laser energy to the clusters, far exceeding that in case of interaction of a laser pulse with a low-density unclustered gas. By the time the laser propagates 1.5 cm through the clustered gas more than 80% of its energy is absorbed. The simulations suggest rapid absorption of energy by the clusters during the initial part of the propagation and the rate of absorption falls off with propagation distance. Also, a pulse with higher initial energy was absorbed much faster than a pulse with lower energy. This efficient absorption of laser energy by the clusters is an important property with respect to the applications. The pulse is frequency shifted as it propagates. This is primarily due to the temporal variation in the cluster complex polarizability leading to a time-varying dielectric constant. Also as the pulse propagates, it develops a moving focus reflected as a kink in the on-axis phase. This, along with the time dependence of polarizability, leads to a redshift in the pulse spectrum.

ACKNOWLEDGMENTS

One of the authors, A. G., would like to thank Professor T. Taguchi for discussions and J. Cooley for help with figures. This work was supported by the National Science Foundation and the U.S. Department of Energy, Office of High Energy Physics.

[1] A. McPherson, T. S. Luk, B. D. Thompson, A. B. Borisov, O. B. Shiryaev, X. Chen, K. Boyer, and C. K. Rhodes, Phys. Rev. Lett. **72**, 1810 (1994).

[2] G. D. Kubiak, L. J. Bernarez, K. D. Krenz, D. J. O'Connell, R. Gutowski, and A. M. M. Todd, in *OSA Trends in Optics and Photonics*, Vol. 4, edited by G. D. Kubiak and D. R. Kania (Optical Society of America, Washington, DC, 1996), pp. 66–71.

[3] Y. L. Shao *et al.*, Phys. Rev. Lett. **77**, 3343 (1996); V. Kumarappan *et al.*, *ibid.* **87**, 085005 (2001).

[4] J. W. G. Tisch, Phys. Rev. A **62**, R41 802 (2000); T. Tajima, Y. Kishimoto, and M. C. Downer, Phys. Plasmas **6**, 3759 (1999).

[5] T. Ditmire, J. Zweiback, V. P. Yanovsky, T. E. Cowan, G. Hays, and K. B. Wharton, Nature (London) **398**, 489 (1999).

[6] I. Alexeev, K. Y. Kim, T. Antonsen, and H. M. Milchberg, Phys. Rev. Lett. **90**, 103402 (2003).

[7] T. Ditmire, R. A. Smith, J. W. G. Tisch, and M. H. R. Hutchinson, Phys. Rev. Lett. **78**, 3121 (1997).

[8] K. Y. Kim, H. Milchberg, V. Kumarappan, I. Alexeev, A. Gupta, and T. M. Antonsen, Bull. Am. Phys. Soc. **48**, 132 (2003), http://www.aps.org/meet/DPP03/baps/abs/S940006.html

[9] B. D. Thompson, A. McPherson, K. Boyer, and C. K. Rhodes, J. Phys. B **27**, 4391 (1994).

[10] C. Rose-Petruck, K. J. Schafer, K. R. Wilson, and C. P. J. Barty, Phys. Rev. A **55**, 1182 (1997).

[11] T. Ditmire, T. Donnelly, A. M. Rubenchik, R. W. Falcone, and M. D. Perry, Phys. Rev. A **53**, 3379 (1996).

[12] J. Zweiback, T. Ditmire, and M. D. Perry, Phys. Rev. A **59**, R3166 (1999).

[13] J. Zweiback, T. Ditmire, and M. D. Perry, Opt. Express **6**, 236 (2000).

[14] H. M. Milchberg, S. J. McNaught, and E. Parra, Phys. Rev. E **64**, 056402 (2001).

[15] K. Y. Kim, I. Alexeev, E. Parra, and H. M. Milchberg, Phys. Rev. Lett. **90**, 023401 (2003).

[16] K. Y. Kim, V. Kumarappan, A. Gupta, T. Antonsen, H. Milchberg, A. Faenov, and T. Pikuz, CLEO/IQEC & PhAST 2004 Conference Program, p. 70.

[17] H.-H. Chu, H.-E. Tsai, Y.-F. Xiao, C.-H. Lee, J.-Y. Lin, J. Wang, and S.-Y. Chen, Phys. Rev. E **69**, 035403(R) (2004).

[18] T. Taguchi, T. Antonsen, and H. M. Milchberg, Phys. Rev. Lett. **92**, 205003 (2004).

[19] M. Eloy, R. Azambuja, J. T. Mendonca, and R. Bingham, Phys. Plasmas **8**, 1084 (2001).

[20] C. Jungreuthmayer, M. Geissler, J. Zanghellini, and T. Brabec, Phys. Rev. Lett. **92**, 133401 (2004).

[21] S. V. Fomichev, S. V. Popruzhenko, D. F. Zartesky, and W.

Becker, J. Phys. B **36**, 3817 (2003).
[22] M. V. Fomyts'kyi, B. N. Breizman, A. V. Arefiev, and C. Chiu, Phys. Plasmas **11**, 3349 (2004).
[23] J. Liu, R. Li, P. Zhu, Z. Xu, and J. Liu, Phys. Rev. A **64**, 033426 (2001).
[24] N. A. Zharova, A. G. Litvak, and V. A. Mironov, JETP Lett. **78**, 619 (2003).
[25] M. Rusek, H. Lagadec, and T. Belinski, Phys. Rev. A **63**, 013203 (2000).
[26] A. Gupta, T. Antonsen, and H. Milchberg, Bull. Am. Phys. Soc. **46**, 201 (2001).
[27] E. Esarey, P. Sprangle, J. Krall, and A. Ting, IEEE J. Quantum Electron. **33**, 1879 (1997).
[28] J. D. Jackson, *Classical Electrodynamics* (Wiley, New York, 1998).
[29] NRL Plasma Formulary.